Phenotypic and Functional Plasticity of Murine Intestinal NKp46+ Group 3 Innate Lymphoid Cells

Thomas Verrier, Naoko Satoh-Takayama, Nicolas Serafini, Solenne Marie, James P Di Santo, Christian A. J. Vosshenrich

Phenotypic and functional plasticity of murine intestinal NKp46^{+} ILC3

Thomas Verrier[1,2,3], Naoko Satoh-Takayama[1,2,4], Nicolas Serafini[1,2], Solenne Marie[1,2], James P. Di Santo[1,2,§] and Christian A.J. Vosshenrich[1,2]

[1]*Innate Immunity Unit, Institut Pasteur, 25 rue du Docteur Roux, 75724 Paris, France*

[2]*Inserm U1223, Paris, France*

[3]*Paris Diderot University, Paris, France*

[4]*Laboratory for Intestinal Ecosystem, RIKEN Center for Integrative Medical Science (IMS), Yokohama, Japan*

[§] To whom correspondence should be addressed:

Innate Immunity Unit

Inserm U1223

Institut Pasteur

25 rue du Docteur Roux

75724 Paris, France

Tel : + 33 1 45 68 86 96

Fax : + 33 1 40 61 35 10

Email : disanto@pasteur.fr

Running title: Fate-mapping gut NKp46^{+} ILC3 subsets

Character count: 37675 (including spaces)

Abstract

Type 3 Innate Lymphoid Cells (ILC3) actively participate in mucosal defense and homeostasis through prompt secretion of IL-17A, IL-22 and IFN-γ. Reports identify two ILC3 lineages : a CCR6^{+}T-bet^{-} subset that appears early in embryonic development and promotes lymphoid organogenesis, and a CCR6^{-}T-bet^{+} subset that emerges after microbial colonization and harbors NKp46^{+} ILC3. Here, we demonstrate that NKp46 expression in ILC3 subset is highly unstable. Cell fate-mapping using *Ncr1*$^{\text{CreGFP}}$ x *Rosa26*$^{\text{RFP}}$ mice revealed the existence of an intestinal RFP^{+} ILC3 subset (*Ncr1*$^{\text{FM}}$) lacking NKp46 expression at the transcript and protein level. *Ncr1*$^{\text{FM}}$ ILC3 produced more IL-22 and were distinguishable from *NKp46*$^{+}$ ILC3 by differential CD117, CD49a, DNAM-1, and surprisingly, CCR6 expression. *Ncr1*$^{\text{FM}}$ ILC3 emerged after birth and persisted in adult mice following broad-spectrum antibiotic treatment. These results identify an unexpected phenotypic instability within NKp46^{+} ILC3 that suggests a major role for environmental signals in tuning ILC3 functional plasticity.

Introduction

Innate lymphoid cells (ILCs) comprise an evolutionarily conserved and related set of innate immune effectors. Three ILC groups can be distinguished on the basis of their transcription factors profiles and cytokine production (1–3). T-bet-expressing ILC1 are involved in responses against viruses, intracellular pathogens and tumors and include Eomes-dependent cytotoxic ILC1 (NK cells) and Eomes-independent ILC1, both of which produce interferon-γ (IFN-γ). ILC2 participate in protection against helminthes and viruses via Gata-3-dependent production of interleukins (IL)-5, IL-13 and amphiregulin, but may also aggravate allergic responses. ILC3 are enriched at mucosal sites, drive lymphoid tissue organogenesis during fetal life, and maintain intestinal homeostasis in adults through IL-22 production downstream of the transcription factor RORγt. Two ILC3 sublineages have been proposed (4, 5): a $CCR6^{+}$T-bet^{-} subset that includes Lymphoid Tissue inducer (LTi) cells, and $CCR6^{-}$T-bet^{+} subset that develops post-natally in response to microbial stimulation and gives rise to cells expressing the natural cytotoxic receptor (NCR) NKp46. These two ILC3 subsets share strong functional similarities (6), but occupy distinct niches (7–10). As such their respective specific versus redundant roles in mucosal defense remain unclear.

While NKp46 crosslinking triggers cytotoxicity in human and mouse NK cells, the functional role for NCR on ILC3 is poorly understood. Cytokine production in human ILC3 can be stimulated by anti-NKp44 antibodies (11) although the ligands that can mimic this activity *in vivo* remain unknown. In the mouse, *Ncr1* ablation (in $Ncr1^{GFP/GFP}$ mice) has little impact on ILC3 homeostasis and cytokine responses to pathogenic *Citrobacter rodentium* are unaffected (12). Modulation of NKp46 expression on NK cells occurs during MCMV infection (13) and may ‘tune’ ILC3

responses in a fashion similar to that proposed for 'licensing' of cytokine and cytotoxic responses of NK cells via NKp46 (14).

To address dynamics of NKp46 expression in mucosal ILC3, we have performed *in vivo* fate-mapping studies using *Ncr1*^{CreGFP} mice (15) that harbor a transgene containing the *Ncr1* proximal promoter driving expression of a Green Fluorescent Protein/Cre-recombinase fusion protein (CreGFP). Analysis of *Ncr1*^{CreGFP} x *Rosa26*^{RFP} mice (in which NKp46-expressing cells are indelibly marked with RFP expression) revealed the existence of an unusual NKp46^{-}GFP^{-}RFP^{+} cells uniquely within the intestinal mucosa. Here we report the phenotypic and functional characterization of these cells (referred to here as '*Ncr1* Fate-Mapped' ILC3 or *Ncr1*^{FM} ILC3) and discuss the potential implications for NKp46 plasticity in mucosal immunity.

Material and Methods

Mice

Tg(Ncr1-cre/EGFP)#Cajv mice (*Ncr1*^{CreGFP}) were generated and crossed to *Rosa26*^{RFP} mice as described (15). *Ncr1*$^{GFP/+}$ mice (16) were the kind gift from O. Mandelboim (Jerusalem, Israel). Unless specified otherwise, adult mice were used between 7 and 13 weeks of age. For E18.5 embryos, mice were co-housed overnight, female mice with a vaginal plug were separated the next day, with embryos considered as E0.5.

Antibiotic treatment

An antibiotic cocktail was used to deplete intestinal commensal microbiota as previously described (4). Ampicillin (1g/L), colistin (1g/L), streptomycin (5g/L) and sucrose (20%; Sigma Aldrich) were diluted into drinking water and then filter sterilized (0.22μm). Plugged female mice were treated with antibiotics; the drinking water was changed each week. Four weeks after birth, pups were weaned and treatment continued until sacrifice 3 weeks later.

Isolation of Lamina Propria Lymphocytes

Small intestine were extracted and perfused with cold RPMI-1640 medium to remove feces. Peyer's patches were removed and the intestine cut open longitudinally, then washed again. Intestine were cut into 1cm pieces and agitated in pre-warmed RPMI-1640 medium (Gibco) containing 10mM EDTA (Sigma-aldrich) at 37°C for 15 min, followed by 15 min wash with RPMI-1640 alone at 37°C. Pieces of intestine were harvested, cut into small pieces and digested in RPMI (Gibco) containing 5% FCS and Collagenase VII (0.75mg/mL; Sigma-Aldrich) (twice for 20 min each). After each extraction, supernatants were collected, filtered (100 μm), pooled and

centrifuged (300g; 10 min). Lymphocytes were enriched by Percoll 80/40% gradient centrifugation. For stimulation, 1-2 x 10^6 cells were incubated at 37°C with IL-1β (R&D;100 ng/ml), IL-2 (Peprotech; 100ng/ml), IL-6 (R&D; 20ng/ml), IL-23 (R&D system; 50ng/mL) in RPMI-1640 medium containing 10% FCS, penicillin (Gibco), streptomycin (Gibco) for 1 hour. PMA (50ng/ml) and ionomycin (500ng/ml) were added together with BD GolgiPlug™ (BD Pharmingen; 555029) for the last 3 hours before analysis of intracellular cytokines by FACS.

Flow cytometry

Cell suspensions were incubated for 40 minutes with cold PBS (Gibco) containing 10% FCS, Fc receptor block (2.4G2), a viability dye (eFluor® 506, eBioscience #65-0866-14) and fluorochrome bound antibodies. To detect intracellular antigens, cells were fixed for 40 minutes with 2% paraformaldehyde followed by a permeabilization/staining step for transcription factors and/or cytokines with the Foxp3 permeabilization kit (eBioscience). The following antibodies were used: CD3 (17A2), CD4 (RM4-5), NK1.1 (PK136), CD127 (A7R34), CD117 (2B8), ROR, IL-22 (IL22JOP), NKp46 (29A1.4), CCR6 (29-2L17), T-bet (ebio4B10), MHC-II (M5/114.15.2), CD49a (Ha31/8), Ki67 (SoIA15), DNAM (10E5). All the samples were acquired on a LSR FORTESSA (BD), and data were analyzed with FlowJo (TreeStar, version 9.8.5 & 10.0.8).

Cell Culture of ILC3

ILC3 from the SI-LP of *Ncr1*$^{GFP/+}$ mice were isolated as CD45^{int} CD90^{hi} NK1.1^{-}, and dissected according to GFP, CD49a and CCR6 expression. Cells were sorted using a FACSAria II (BD) and were cultured on OP9 or OP9-DL1 stromal cells (kind gift of

A. Cumano, Institut Pasteur) in IMDM (Lonza) containing 10% FCS, 1× penicillin/streptomycin (Gibco), and 60μM 2-mercaptoethanol (Sigma-Aldrich), rIL-7 (20ng/mL) and rSCF (20ng/mL). 2 and 4 days later, cells were harvested and stained (as stated above) for CD45, CD90, NK1.1, CD49a, CCR6, NKp46. Expressions (along with GFP) of these marker were then analyzed by FACS.

Statistical analysis

Data were compiled and analyzed with Graphpad Prism software (version 6). Paired and unpaired Student's t-test were used to determine statistical differences between groups. All graphs display mean + S.E.M., p values < 0.05 were considered significant.

Results

In vivo fate-mapping of Ncr1^{+} innate lymphoid cell subsets

Ncr1^{CreGFP} mice express a Cre-recombinase-GFP fusion protein under the control of a minimal Ncr1 promoter and have been shown to faithfully report GFP expression and Cre recombinase activity in known NKp46^{+} cells, including NK cells, ILC1 and NKp46^{+} ILC3 (15). We crossed *Ncr1*^{CreGFP} mice with *Rosa26*^{RFP} Cre reporter mice in order to genetically mark NKp46^{+} cells (RFP) that would allow us to investigate the stability of NKp46 expression (Supplemental Figure 1A). In agreement with our previous results (15) , RFP^{+} cells isolated from bone marrow, spleen, lymph nodes, salivary glands, liver, and lung of *Ncr1*^{CreGFP} x *Rosa26*^{RFP} mice uniformly expressed cell surface NKp46 and NK1.1^{+} (Figure 1A, Supplemental Figure 1B) thus identifying these RFP^{+} cells as group 1 ILC.

In contrast, RFP^{+} cells isolated from gut-associated tissues, including small intestine lamina propria (SI-LP) and Peyer's Patches (PP) were clearly different with a clear fraction of cells lacking cell surface NKp46 and GFP expression (Figure 1A, and Supplemental Figure 1C). These NKp46^{-}GFP^{-} cells represented about 30% of the total RFP^{+} cells within the SI-LPL or PP, were uniformly NK1.1^{-} and highly expressed RORγt (Figure 1A and Supplemental Figure 1C). As RORγt and Eomes expression in CD3^{-}CD19^{-} intestinal cells are mutually exclusive (Supplemental Figure 1D), the NKp46^{-}GFP^{-}RFP^{+} cells are not related to Eomes^{+} ILC1. As such, RFP^{+}NKp46^{-}GFP^{-} cells appeared as "ex-NKp46-ILC3' that had lost NKp46 expression. We purified NKp46^{-}GFP^{-}RFP^{+} cells and confirmed that they significantly lacked mRNA for *Ncr1* that encodes NKp46 (Figure 1C). We refer to the NKp46^{-}GFP^{-}RFP^{+} cells in *Ncr1*^{CreGFP} x *Rosa26*^{RFP} mice as '*Ncr1* Fate-Mapped' ILC3 or

167 *Ncr1*^{FM} ILC3. *Ncr1*^{FM} ILC3 were not detected in the large intestine under steady-state
168 conditions (Supplemental Figure 1C).

169 Since NKp46 expression levels are lower (yet overlapping) in ILC3 compared
170 to NK/ILC1, a clear separation of these subsets by antibody staining alone is not
171 possible. We therefore examined NKp46 cell surface versus GFP expression in
172 RORγt^{+} ILC3 within total RFP^{+} cells (Figure 1B). This approach allowed us to
173 unambiguously identify *Ncr1*^{FM} ILC3 as NKp46^{-}GFP^{-}RFP^{+} cells within the RORγt^{+}
174 gate. ILC3 subsets co-express CD117 (c-kit) and CD127 (IL-7Rα), albeit at varying
175 levels (Figure 1D). For example, previous studies have shown that CCR6^{+} ILC3 were
176 CD117^{hi} CD127^{hi} as opposed to NKp46^{+}CCR6^{-} ILC3 that express lower CD117 and
177 CD127 levels (4). We found that *Ncr1*^{FM} ILC3 expressed significantly higher levels
178 of CD127 and CD117 as compared to NKp46^{+} ILC3 (Figure 1E). Further analyses
179 revealed that a fraction of *Ncr1*^{FM} ILC3 expressed CCR6 (Figure 1F). On average, we
180 found 4 x 10^{4} *Ncr1*^{FM} ILC3 in the SI-LP from *Ncr1*^{CreGFP} x *Rosa26*^{RFP} mice, of which
181 33.5 ± 5.7 % expressed CCR6 (Figure 1G). Thus, CCR6^{+} *Ncr1*^{FM} ILC3 represented
182 about 10% of total CCR6^{+} ILC3 pool (Figure 1G). Some of these CCR6^{+} *Ncr1*^{FM}
183 ILC3 expressed major histocompatibilty complex class II molecules at the cell surface
184 (Supplemental Figure 2A) but these represented a minute fraction of total MHC class
185 II^{+} ILC3 pool. The remaining *Ncr1*^{FM} ILC3 lacked CCR6 and CD4 expression
186 (Supplemental Figure 2B) and would be contained within the 'double negative'
187 (NKp46^{-}CCR6^{-}) or 'DN' ILC3 gate. Within the total DN ILC3 population, *Ncr1*^{FM}
188 ILC3 accounted for about 17% of cells. Thus, a substantial fraction of previously
189 identified DN ILC3 are in fact, *Ncr1*^{FM} ILC3 that have lost NKp46 expression.

190 As some T cells express NKp46 (17, 18) or RORγt (19, 20), we assessed
191 whether *Ncr1*^{FM} ILC3 could represent a peculiar T cell subset that had lost surface

192 expression of CD3 and NKp46. However, neither NKp46^{+}RFP^{+} nor NKp46^{-}RFP^{+}
193 ILC3 expressed cell surface CD5 or intracellular CD3 protein (Figure 1H).
194 Importantly, intracellular NKp46 protein was not detected in *Ncr1*^{FM} ILC3, ruling out
195 that the loss of cell surface NKp46 was due to the protein internalization (Figure 1H).
196 Taken together, analyses of *Ncr1*^{CreGFP} x *Rosa26*^{RFP} mice provide clear
197 evidence for an intestinal ILC3 subset that has modulated NKp46 expression at both
198 the protein and transcriptional level.
199
200 *Functional capacities of Ncr1*^{FM} ILC3
201 *Ncr1*^{FM} ILC3 did not stain for Ki67 suggesting that they were primarily resting
202 cells (Figure 2A, B). Given that one major ILC3 function is the production of IL-22,
203 we assessed whether *Ncr1*^{FM} ILC3 were able to produce this cytokine upon
204 stimulation *in vitro*. Of note, IL-22 protein was readily detectable in both *Ncr1*$^{+}$ ILC3
205 and *Ncr1*^{FM} ILC3 even without IL-23 stimulation (Figure 2C), however, steady-state
206 IL-22 production by *Ncr1*^{FM} ILC3 was significantly greater than that of *Ncr1*$^{+}$ ILC3
207 on a population level as well as on a per cell basis (Figure 2D, E). Nevertheless, upon
208 stimulation with IL-23, both *Ncr1*$^{+}$ ILC3 and *Ncr1*^{FM} ILC3 produced similar levels of
209 IL-22 (Figures 2C-E). These results suggest that *Ncr1*^{FM} ILC3 may have received
210 activating signals *in situ*; such pathways might also be involved in NKp46 down-
211 modulation, although this remains speculative.
212 We explored the cytokine production capacities of *Ncr1*^{FM} ILC3 using various
213 stimuli. Only group 1 ILC (NKp46^{+}GFP^{+}RORγt^{-}) cells produced IFNγ upon
214 stimulation with IL-2, IL-12, and IL-18 (Figure 2F), while both *Ncr1*$^{+}$ ILC3 and
215 *Ncr1*^{FM} ILC3 produced IL-22 under these conditions (Figure 2F). Interestingly,
216 around 1 out of 4 of the IL-22 producing *Ncr1*$^{+}$ ILC3 and *Ncr1*^{FM} ILC3 also produced

GM-CSF (Supplemental Figure 3A). The frequencies of both IL-22 producing cells and IL-22/GM-CSF producing cells increased when stimulated with a cocktail consisting of IL-1β, IL-2, IL-6, IL-23 and PMA/ionomycin (Figure 2F and Supplemental Figure 3A). Under these conditions, around half of IL-22$^+$ *Ncr1*$^+$ ILC3 produced IFNγ whereas *Ncr1*^{FM} ILC3 did not (Supplemental Figure 3A). RFP$^+$ cells failed to produce IL-17A after stimulation (Supplemental Figure 3B). Consistent with their ability to produce IFNγ, *Ncr1*$^+$ ILC3 express T-bet (Figure 2G) and require this transcription factor for development (5, 22). In contrast, *Ncr1*^{FM} ILC3 expressed significantly less T-bet protein when compared with NK1.1$^+$ NK/ILC1 or with *Ncr1*$^+$ ILC3 (Figure 2G and H).

Ontogeny of Ncr1^{FM} ILC3 *and the role of microbiota*

We next explored at what stage *Ncr1*^{FM} ILC3 emerged during ontogeny. CCR6$^+$ ILC3 have been detected as early as E13.5 (23). However, only few RFP$^+$ cells were found at E18.5 (Figure 3A) and these cells uniformly expressed NK1.1 (Supplemental Figure 4). One week after birth, RFP$^+$NK1.1$^-$ cells were apparent, the majority of which were *Ncr1*^{FM} ILC3 (Figure 3B), which indicates that NKp46 expression was initiated, but not maintained in these RFP$^+$ cells. Interestingly, *Ncr1*^{FM} ILC3 exhibited higher IL-22 production capacity at this stage, both under steady state conditions, and after IL-23 stimulation (Figure 3C), the latter contrasting with the results obtained in adult mice (Figure 2C, D). We also noted an age-dependent decrease in the frequency of *Ncr1*^{FM} among total ILC3 (13.2 ± 2.9 % and 9.4 ± 2.7% of total ILC3 in 1 week and 7 week-old mice, respectively). This might point to a specific function of these cells during the early postnatal period.

IL-23 driven T-bet expression in CCR6$^-$ ILC3 was shown to be induced by microbiota resulting in the generation of NKp46$^+$ ILC3 (5). As *Ncr1*^{FM} ILC3 emerged after birth and increased with age (4), we hypothetized that microbiota might also regulate *Ncr1*^{FM} ILC3 homeostasis. To address this point, we treated *Ncr1*^{CreGFP} x *Rosa26*^{RFP} mice with broad-spectrum antibiotics that have been shown to largely ablate commensal microbial communities (9). As expected (9), CD3$^+$ RORγt$^+$ T cells were decreased after antibiotic treatment (Figure 3D). In contrast, we did not observe any changes in proportions of *Ncr1*$^+$ ILC3 or *Ncr1*^{FM} ILC3 (Figure 3E, F). These results indicate that antibiotic-sensitive microbiota are not a major driving force in shaping *Ncr1*^{FM} ILC3 homeostasis in adult mice. Nevertheless, future studies using germ-free *Ncr1*^{CreGFP}*Rosa26*^{RFP} mice should be performed to confirm whether homeostasis of the *Ncr1*^{FM} ILC3 subset is microbiota independent.

CD49a and CD226 expression by ILC3 subsets

CD49a (encoded by *Itga1*) is highly expressed by Eomes-independent hepatic ILC1 (DX5$^-$NK1.1$^+$ cells) but is largely absent on Eomes$^+$ DX5$^+$ NK cells (24, 25). Subsequently, CD49a has been proposed as surface marker to identify ILC1 in various organs (26). As both ILC1 and NKp46$^+$ ILC3 require T-bet for their development (5, 22, 25, 26), we assessed whether CD49a might also be differentially expressed by intestinal ILC3 subsets. We found that CD49a was uniformly expressed by NKp46$^+$ and a subset of DN (NKp46$^-$CCR6$^-$) ILC3 (Figure 4A). Importantly, CD49a was co-expressed with T-bet in both populations, while CCR6 and CD49a expression were mutually exclusive (Figure 4A) consistent with previous transcriptomic analysis of ILC3 subsets (6). Consequently, all *Ncr1*$^+$ ILC3 expressed

CD49a (Figure 4B). In contrast, only a fraction of *Ncr1*^{FM} ILC3 stained positive for this marker (Figure 4B).

We next examined whether DNAX accessory molecule-1 (DNAM-1 or CD226) was expressed by *Ncr1*^{FM} ILC3. CD226 identifies NK/ILC1 subsets with enhanced IFNγ production (27). DNAM ligands - CD112 and CD155 - are expressed by DCs and other cells (28), and CD226-CD155 interactions have been shown to be involved in NK-DC 'crosstalk' (29). CD226 expression varied on ILC3 subsets: it was expressed at high levels by all CCR6^{-} ILC3 (Figure 4C), while the majority of CCR6^{+} ILC3 expressed intermediate levels, with a small fraction of CCR6^{+} ILC3 being CD226^{-} (Figure 4C). We found that *Ncr1*$^{+}$ ILC3 expressed high levels of CD226, while *Ncr1*^{FM} ILC3 contained CD226^{hi} and CD226^{int} cells (Figure 4C). High level CD226 expression by *Ncr1*^{FM} ILC3 was associated with CD49a expression (Figure 4C), while CD49a^{-} *Ncr1*^{FM} ILC3 expressed intermediate levels of CD226 and harbored the CCR6^{+} subset (Figure 4C). Together these data reveal a cluster of markers (NKp46, CD49a, CD226) that are highly expressed by T-bet^{+} ILC3 and are down-regulated in *Ncr1*^{FM} ILC3.

Signals that modulate NKp46 expression on intestinal ILC3

Membrane bound and soluble factors regulate NK cell receptor expression. Concerning NCRs, Notch has been proposed as a key positive regulator for mucosal ILC3 in mice (22), while TGF-β can modulate human NKp30 expression *in vitro* (30). NKp46 expression is reduced in cancer patients (31) and during Influenza and HIV infection (31–33). To begin to investigate the signals that might be involved in the regulation of NKp46 expression in *Ncr1*^{FM} ILC3, we used *Ncr1*$^{GFP/+}$ (16) mice in which one *Ncr1* allele harbors a fluorescent reporter generating high GFP expression

290 by all NKp46^{+} cells. We then isolated CD49a^{+}GFP^{+}, CD49a^{+}GFP^{-}, and CCR6^{+} ILC3
291 subsets and monitored GFP expression after cell culture on stromal cells that
292 differentially expressed Notch ligands (22). We could detect a significant decrease in
293 the GFP expression level (mean fluorescence intensity) between day 2 and day 4 by
294 CD49a^{+} GFP^{+} cells cultured on OP9 stromal cells, whereas GFP expression remained
295 constant on OP9 DL1 cells (Figure 4D). Addition of TGF-β accelerated GFP
296 downregulation in CD49a^{+} GFP^{+} cells cultured on OP9 but not OP9 DL1 (Figure 4D).
297 In contrast, GFP expression was not induced in cultured CCR6^{+} or CD49a^{+} GFP^{-} ILC3
298 and no changes in CD49a or CCR6 expression were observed under any conditions
299 (Supplemental Figure 5). These results suggest that TGF-β and Notch-derived signals
300 regulate NKp46 expression in cultured *Ncr1*$^{+}$ ILC3 and may be involved in the
301 maintenance of NKp46 expression on *Ncr1*$^{+}$ ILC3 or the generation of *Ncr1*^{FM} ILC3.

Discussion

Using *in vivo* fate-mapping, we have identified an unusual subset of intestinal ILC3 that have lost previous NKp46 expression; these 'ex-NKp46 ILC3' are denoted *Ncr1*^{FM} ILC3. As a result, a fraction of 'DN' (CD4^{-}NKp46^{-}) ILC3 are derived from *Ncr1*$^{+}$ ILC3 and demonstrate that the NKp46^{+} ILC3 is not a stable or determinant phenotype. Our results also indicate that the 'DN' ILC3 subset is heterogeneous and show that at least two pathways are involved in the generation of this population.

Interestingly, a small subset of *Ncr1*^{FM} ILC3 express CCR6, thus resembling LTi-like cells. It is a currently not clear whether CCR6^{+} ILC3 represent a stable lineage (21). Constantinides et al. identified early ILC precursors using *Zbtb16*^{CreGFP} mice and through fate-mapping, showed that while most NKp46^{+} ILC3 were derived from *Zbtb16*-expressing precursors, a minor fraction of CCR6^{+} ILC3 were also fate-mapped (21). Conceivably, the small subset of CCR6^{+} *Ncr1*^{FM} ILC3 we identified might correspond to (or be contained within) the CCR6^{+} *Zbtb16*-derived ILC3 population (21). Since NKp46^{+} ILC3 are CCR6^{-}, this receptor appears to be induced on a fraction of *Ncr1*^{FM} ILC3, possibly in response to environmental cues. As such, the generation of CCR6^{+} *Ncr1*^{FM} ILC3 may allow for a specific postnatal positioning of these IL-22 producing ILC3 cells within the intestine.

We found that CD49a and CD226 are differentiatlly expressed on intestinal ILC3. *Ncr1*$^{+}$ ILC3 express both markers, while *Ncr1*^{FM} ILC3 have reduced levels. As CD49a and CCR6 were exclusively expressed by *Ncr1*^{FM} ILC3, we propose the following sequence: RFP^{+}NKp46^{+}CD49a^{+}CD226^{hi}CCR6^{-} -> RFP^{+}NKp46^{-} CD49a^{+}CD226^{hi}CCR6^{-} -> RFP^{+}NKp46^{-}CD49a^{-}CD226^{int}CCR6^{+}. The change in CD49a and CCR6 expression might allow for a differential localization of *Ncr1*$^{+}$ and *Ncr1*^{FM} ILC3 within the tissue enabling them to exert their function in the correct

cellular context. Indeed, *Ncr1*^{FM} ILC3s displayed spontaneous production of IL-22 suggesting that they may have received stimulatory signals *in situ*. Further studies on the localization of *Ncr1*$^{+}$ and *Ncr1*^{FM} ILC3 should provide important insights into the specific roles for these ILC subsets in immune homeostasis.

Previous work has revealed that under the influence of environmental cues ILC3 acquire the expression of T-bet and concomitant ability to produce IFNγ (34). T-bet upregulation is associated with loss of RORγt expression and IL-22 production capabilities, allowing ILC3 to acquire an ILC1-like phenotype ("ex-ILC3" ILC1). In contrast, *Ncr1*^{FM} ILC3 do not show signs of ILC1-like plasticity. They retain characteristics of ILC3 (RORγt^{+}, IL-22 production) in naïve mice and when stimulated in vitro. Furthermore, *Ncr1*^{FM} ILC3 expressed lower levels of T-bet than *Ncr1*$^{+}$ ILC3 and were unable to produce IFNγ. However, similar to *Ncr1*$^{+}$ ILC3, they can produce GM-CSF. Whether *Ncr1*^{FM} ILC3 show further plastic features with resultant loss of RORγt expression (similar to this ILC3 to ILC1 differentiation) is not known. Of note, our analyses demonstrated that all RFP^{+} group 1 ILC in *Ncr1*^{CreGFP} x *Rosa26*^{RFP} mice co-express NK1.1 and NKp46. Thus, if such a plasticity (*Ncr1*^{FM} ILC3 to ILC1) would occur, it would involve concomitant upregulation of NKp46 and NK1.1 by those cells, rendering them indistinguishable from "normal" group 1 ILC.

Taken together, NKp46 modulation in ILC3 likely reflects an intrinsic program influenced by environmental cues. AhR activation by dietary ligands may explain higher CD117 and IL-22 expression in *Ncr1*^{FM} (35), while cellular partners that emerge after birth such as monocytes derived CX3CR1^{+} macrophages may stabilize NKp46 expression by providing Notch ligands (36). To balance their function, TGF-β might dampens an ILC3 pro-inflammatory program dependent on NKp46 expression. Remarkably, NKp46^{+} ILC3 are the only immune cell to express

352 simultaneously Gata-3, RORγt and T-bet. The interplay between these transcription
353 factor in ILC3 differentiation is complex and NKp46 expression appears tightly
354 controlled by Gata-3 and T-bet (37). As such, relative amounts of these transcription
355 factors, balanced by extrinsic signals, might finely tune the emergence and the
356 function of *Ncr1*$^{+}$ ILC3 and their transition to *Ncr1*^{FM} ILC3.
357

Acknowledgements

We thank Ana Cumano (Institut Pasteur) for the gift of OP9 stromal cells, Ofer Mandelboim for *Ncr1*^{GFP} mice and Hans-Jorg Fehling for *Rosa26*^{RFP} mice. TV is supported by a PhD Training grants from the French government and the Ligue Nationale Contre le Cancer (LNCC). This work is supported by grants from the Institut Pasteur, Inserm, and LNCC as an 'Equipe Labelisée'.

Conflict of Interest Statement

JD is a founder and stakeholder in AXENIS (Paris, France). The other authors declare no conflict of interest.

368 **References**

369

370 1. Sonnenberg, G. F., and D. Artis. 2015. Innate lymphoid cells in the initiation,
371 regulation and resolution of inflammation. *Nat. Med.* 21: 698–708.

372

373 2. Eberl, G., M. Colonna, J. P. Di Santo, and A. N. J. McKenzie. 2015. Innate
374 lymphoid cells. Innate lymphoid cells: a new paradigm in immunology. *Science* 348:
375 aaa6566.

376

377 3. Serafini, N., C. A. J. Vosshenrich, and J. P. Di Santo. 2015. Transcriptional
378 regulation of innate lymphoid cell fate. *Nat. Rev. Immunol.* 15: 415–428.

379

380 4. Sawa, S., M. Cherrier, M. Lochner, N. Satoh-Takayama, H. J. Fehling, F. Langa, J.
381 P. Di Santo, and G. Eberl. 2010. Lineage relationship analysis of RORgammat+
382 innate lymphoid cells. *Science* 330: 665–669.

383

384 5. Klose, C. S. N., E. A. Kiss, V. Schwierzeck, K. Ebert, T. Hoyler, Y. d'Hargues, N.
385 Göppert, A. L. Croxford, A. Waisman, Y. Tanriver, and A. Diefenbach. 2013. A T-
386 bet gradient controls the fate and function of CCR6-RORγt+ innate lymphoid cells.
387 *Nature* 494: 261–265.

388

389 6. Robinette, M. L., A. Fuchs, V. S. Cortez, J. S. Lee, Y. Wang, S. K. Durum, S.
390 Gilfillan, M. Colonna, and Immunological Genome Consortium. 2015.
391 Transcriptional programs define molecular characteristics of innate lymphoid cell
392 classes and subsets. *Nat. Immunol.* 16: 306–317.

393

394 7. Satoh-Takayama, N., C. A. J. Vosshenrich, S. Lesjean-Pottier, S. Sawa, M.
395 Lochner, F. Rattis, J.-J. Mention, K. Thiam, N. Cerf-Bensussan, O. Mandelboim, G.
396 Eberl, and J. P. Di Santo. 2008. Microbial flora drives interleukin 22 production in
397 intestinal NKp46+ cells that provide innate mucosal immune defense. *Immunity* 29:
398 958–970.

399

400 8. Luci, C., A. Reynders, I. I. Ivanov, C. Cognet, L. Chiche, L. Chasson, J.
401 Hardwigsen, E. Anguiano, J. Banchereau, D. Chaussabel, M. Dalod, D. R. Littman, E.
402 Vivier, and E. Tomasello. 2009. Influence of the transcription factor RORgammat on
403 the development of NKp46+ cell populations in gut and skin. *Nat. Immunol.* 10: 75–
404 82.

405

406 9. Sawa, S., M. Lochner, N. Satoh-Takayama, S. Dulauroy, M. Bérard, M.
407 Kleinschek, D. Cua, J. P. Di Santo, and G. Eberl. 2011. RORγt+ innate lymphoid
408 cells regulate intestinal homeostasis by integrating negative signals from the
409 symbiotic microbiota. *Nat. Immunol.* 12: 320–326.

410

411 10. Satoh-Takayama, N., N. Serafini, T. Verrier, A. Rekiki, J.-C. Renauld, G. Frankel,
412 and J. P. Di Santo. 2014. The chemokine receptor CXCR6 controls the functional
413 topography of interleukin-22 producing intestinal innate lymphoid cells. *Immunity* 41:
414 776–788.

415

416 11. Glatzer, T., M. Killig, J. Meisig, I. Ommert, M. Luetke-Eversloh, M. Babic, D.
417 Paclik, N. Blüthgen, R. Seidl, C. Seifarth, J. Gröne, M. Lenarz, K. Stölzel, D.

418 Fugmann, A. Porgador, A. Hauser, A. Karlas, and C. Romagnani. 2013. RORγt^{+}
419 innate lymphoid cells acquire a proinflammatory program upon engagement of the
420 activating receptor NKp44. *Immunity* 38: 1223–1235.
421
422 12. Satoh-Takayama, N., L. Dumoutier, S. Lesjean-Pottier, V. S. G. Ribeiro, O.
423 Mandelboim, J.-C. Renauld, C. A. J. Vosshenrich, and J. P. Di Santo. 2009. The
424 natural cytotoxicity receptor NKp46 is dispensable for IL-22-mediated innate
425 intestinal immune defense against Citrobacter rodentium. *J. Immunol.* 183: 6579–
426 6587.
427
428 13. Sun, J. C., J. N. Beilke, N. A. Bezman, and L. L. Lanier. 2011. Homeostatic
429 proliferation generates long-lived natural killer cells that respond against viral
430 infection. *J. Exp. Med.* 208: 357–368.
431
432 14. Narni-Mancinelli, E., B. N. Jaeger, C. Bernat, A. Fenis, S. Kung, A. De Gassart,
433 S. Mahmood, M. Gut, S. C. Heath, J. Estellé, E. Bertosio, F. Vely, L. N. Gastinel, B.
434 Beutler, B. Malissen, M. Malissen, I. G. Gut, E. Vivier, and S. Ugolini. 2012. Tuning
435 of natural killer cell reactivity by NKp46 and Helios calibrates T cell responses.
436 *Science* 335: 344–348.
437
438 15. Merzoug, L. B., S. Marie, N. Satoh-Takayama, S. Lesjean, M. Albanesi, H.
439 Luche, H. J. Fehling, J. P. Di Santo, and C. A. J. Vosshenrich. 2014. Conditional
440 ablation of NKp46+ cells using a novel Ncr1(greenCre) mouse strain: NK cells are
441 essential for protection against pulmonary B16 metastases. *Eur. J. Immunol.* 44:
442 3380–3391.

16. Gazit, R., R. Gruda, M. Elboim, T. I. Arnon, G. Katz, H. Achdout, J. Hanna, U. Qimron, G. Landau, E. Greenbaum, Z. Zakay-Rones, A. Porgador, and O. Mandelboim. 2006. Lethal influenza infection in the absence of the natural killer cell receptor gene Ncr1. *Nat. Immunol.* 7: 517–523.

17. Yu, J., T. Mitsui, M. Wei, H. Mao, J. P. Butchar, M. V. Shah, J. Zhang, A. Mishra, C. Alvarez-Breckenridge, X. Liu, S. Liu, A. Yokohama, R. Trotta, G. Marcucci, D. M. Benson, T. P. Loughran, S. Tridandapani, and M. A. Caligiuri. 2011. NKp46 identifies an NKT cell subset susceptible to leukemic transformation in mouse and human. *J. Clin. Invest.* 121: 1456–1470.

18. Stewart, C. A., T. Walzer, S. H. Robbins, B. Malissen, E. Vivier, and I. Prinz. 2007. Germ-line and rearranged Tcrd transcription distinguish bona fide NK cells and NK-like γδ T cells. *Eur. J. Immunol.* 37: 1442–1452.

19. Martin, B., K. Hirota, D. J. Cua, B. Stockinger, and M. Veldhoen. 2009. Interleukin-17-producing gammadelta T cells selectively expand in response to pathogen products and environmental signals. *Immunity* 31: 321–330.

20. Rachitskaya, A. V., A. M. Hansen, R. Horai, Z. Li, R. Villasmil, D. Luger, R. B. Nussenblatt, and R. R. Caspi. 2008. Cutting edge: NKT cells constitutively express IL-23 receptor and RORgammat and rapidly produce IL-17 upon receptor ligation in an IL-6-independent fashion. *J. Immunol.* 180: 5167–5171.

468 21. Constantinides, M. G., B. D. McDonald, P. A. Verhoef, and A. Bendelac. 2014. A
469 committed precursor to innate lymphoid cells. *Nature* 508: 397–401.
470
471 22. Rankin, L. C., J. R. Groom, M. Chopin, M. J. Herold, J. A. Walker, L. A. Mielke,
472 A. N. J. McKenzie, S. Carotta, S. L. Nutt, and G. T. Belz. 2013. The transcription
473 factor T-bet is essential for the development of NKp46+ innate lymphocytes via the
474 Notch pathway. *Nat. Immunol.* 14: 389–395.
475
476 23. van de Pavert, S. A., M. Ferreira, R. G. Domingues, H. Ribeiro, R. Molenaar, L.
477 Moreira-Santos, F. F. Almeida, S. Ibiza, I. Barbosa, G. Goverse, C. Labão-Almeida,
478 C. Godinho-Silva, T. Konijn, D. Schooneman, T. O'Toole, M. R. Mizee, Y. Habani,
479 E. Haak, F. R. Santori, D. R. Littman, S. Schulte-Merker, E. Dzierzak, J. P. Simas, R.
480 E. Mebius, and H. Veiga-Fernandes. 2014. Maternal retinoids control type 3 innate
481 lymphoid cells and set the offspring immunity. *Nature* 508: 123–127.
482
483 24. Peng, H., X. Jiang, Y. Chen, D. K. Sojka, H. Wei, X. Gao, R. Sun, W. M.
484 Yokoyama, and Z. Tian. 2013. Liver-resident NK cells confer adaptive immunity in
485 skin-contact inflammation. *J. Clin. Invest.* 123: 1444–1456.
486
487 25. Daussy, C., F. Faure, K. Mayol, S. Viel, G. Gasteiger, E. Charrier, J. Bienvenu, T.
488 Henry, E. Debien, U. A. Hasan, J. Marvel, K. Yoh, S. Takahashi, I. Prinz, S. de
489 Bernard, L. Buffat, and T. Walzer. 2014. T-bet and Eomes instruct the development
490 of two distinct natural killer cell lineages in the liver and in the bone marrow. *J. Exp.*
491 *Med.* 211: 563–577.
492

493 26. Klose, C. S. N., M. Flach, L. Möhle, L. Rogell, T. Hoyler, K. Ebert, C. Fabiunke,
494 D. Pfeifer, V. Sexl, D. Fonseca-Pereira, R. G. Domingues, H. Veiga-Fernandes, S. J.
495 Arnold, M. Busslinger, I. R. Dunay, Y. Tanriver, and A. Diefenbach. 2014.
496 Differentiation of type 1 ILCs from a common progenitor to all helper-like innate
497 lymphoid cell lineages. *Cell* 157: 340–356.
498
499 27. Martinet, L., L. Ferrari De Andrade, C. Guillerey, J. S. Lee, J. Liu, F. Souza-
500 Fonseca-Guimaraes, D. S. Hutchinson, T. B. Kolesnik, S. E. Nicholson, N. D.
501 Huntington, and M. J. Smyth. 2015. DNAM-1 expression marks an alternative
502 program of NK cell maturation. *Cell Rep.* 11: 85–97.
503
504 28. Pende, D., R. Castriconi, P. Romagnani, G. M. Spaggiari, S. Marcenaro, A.
505 Dondero, E. Lazzeri, L. Lasagni, S. Martini, P. Rivera, A. Capobianco, L. Moretta, A.
506 Moretta, and C. Bottino. 2006. Expression of the DNAM-1 ligands, Nectin-2
507 (CD112) and poliovirus receptor (CD155), on dendritic cells: relevance for natural
508 killer-dendritic cell interaction. *Blood* 107: 2030–2036.
509
510 29. Seth, S., A.-M. Georgoudaki, B. J. Chambers, Q. Qiu, E. Kremmer, M. K. Maier,
511 N. Czeloth, I. Ravens, R. Foerster, and G. Bernhardt. 2009. Heterogeneous expression
512 of the adhesion receptor CD226 on murine NK and T cells and its function in NK-
513 mediated killing of immature dendritic cells. *J. Leukoc. Biol.* 86: 91–101.
514
515 30. Castriconi, R., C. Cantoni, M. Della Chiesa, M. Vitale, E. Marcenaro, R. Conte,
516 R. Biassoni, C. Bottino, L. Moretta, and A. Moretta. 2003. Transforming growth
517 factor beta 1 inhibits expression of NKp30 and NKG2D receptors: consequences for

518 the NK-mediated killing of dendritic cells. *Proc. Natl. Acad. Sci. U. S. A.* 100: 4120–
519 4125.
520
521 31. Fauriat, C., S. Just-Landi, F. Mallet, C. Arnoulet, D. Sainty, D. Olive, and R. T.
522 Costello. 2007. Deficient expression of NCR in NK cells from acute myeloid
523 leukemia: Evolution during leukemia treatment and impact of leukemia cells in
524 NCRdull phenotype induction. *Blood* 109: 323–330.
525
526 32. Jost, S., J. Reardon, E. Peterson, D. Poole, R. Bosch, G. Alter, and M. Altfeld.
527 2011. Expansion of 2B4+ natural killer (NK) cells and decrease in NKp46+ NK cells
528 in response to influenza. *Immunology* 132: 516–526.
529
530 33. Parsons, M. S., C.-C. Tang, S. Jegaskanda, R. J. Center, A. G. Brooks, I. Stratov,
531 and S. J. Kent. 2014. Anti-HIV antibody-dependent activation of NK cells impairs
532 NKp46 expression. *J. Immunol.* 192: 308–315.
533
534 34. Vonarbourg, C., A. Mortha, V. L. Bui, P. P. Hernandez, E. A. Kiss, T. Hoyler, M.
535 Flach, B. Bengsch, R. Thimme, C. Hölscher, M. Hönig, U. Pannicke, K. Schwarz, C.
536 F. Ware, D. Finke, and A. Diefenbach. 2010. Regulated expression of nuclear
537 receptor RORγt confers distinct functional fates to NK cell receptor-expressing
538 RORγt(+) innate lymphocytes. *Immunity* 33: 736-751.
539
540 35. Zelante, T., R. G. Iannitti, C. Cunha, A. De Luca, G. Giovannini, G. Pieraccini, R.
541 Zecchi, C. D'Angelo, C. Massi-Benedetti, F. Fallarino, A. Carvalho, P. Puccetti, and
542 L. Romani. 2013. Tryptophan catabolites from microbiota engage aryl hydrocarbon
543 receptor and balance mucosal reactivity via interleukin-22. *Immunity* 39: 372–385.

544

545 36. Bain, C. C., A. Bravo-Blas, C. L. Scott, E. Gomez Perdiguero, F. Geissmann, S.
546 Henri, B. Malissen, L. C. Osborne, D. Artis, and A. M. Mowat. 2014. Constant
547 replenishment from circulating monocytes maintains the macrophage pool in the
548 intestine of adult mice. *Nat. Immunol.* 15: 929–937.

549

550 37. Zhong, C., K. Cui, C. Wilhelm, G. Hu, K. Mao, Y. Belkaid, K. Zhao, and J. Zhu.
551 2015. Group 3 innate lymphoid cells continuously require the transcription factor
552 GATA-3 after commitment. *Nat. Immunol.* doi:10.1038/ni.3318.

553

554

555

556

Figure Legends

Figure 1. An unusual 'ex-NKp46' ILC3 subset in the small intestine. (**A**) Analysis of NK1.1, RORγt and NKp46 expression in RFP^+ cells from the indicated organs in *Ncr1*^{CreGFP} x *Rosa26*^{RFP} mice. First column displayed was gated on alive $CD45^+$ RFP^+ cells. SI-LP : Small Intestine Lamina Propria. (**B**) Gating strategy used to identify RFP^+ $NKp46^-$ GFP^- ILC3 in small intestine lamina propria lymphocytes from *Ncr1*^{CreGFP} x *Rosa26*^{RFP} mice. $CD4^+$ LTi cells ($CD3^-$ $CD127^+$ $ROR\gamma t^+$ $CD4^+$) were used as a control to set the negative gate (NKp46 vs GFP). (**C**) Ncr1 mRNA expression levels by sorted intestinal populations: NK1.1+ - CD3-CD45.2+NK1.1+NKp46+GFP+RFP+; Ncr1+ - CD3-CD45.2intCD90.2hiCD117+NK1.1-NKp46+GFP+RFP+; Ncr1FM – CD3-CD45.2intCD90.2hiCD117+NK1.1-NKp46-GFP-RFP+; CD4+ LTi – CD3-CD45.2intCD90.2hiCD117+NK1.1-NKp46-RFP-CD4+. (**D**) Representative FACS plot of CD127 versus CD117 in RFP^+ $NK1.1^-$ cells. (**E**) Expression levels (MFI) of CD127 (left) and CD117 (right) by the indicated populations measured by FACS. (**F**) Representative FACS plot of NKp46, GFP, RFP and CCR6 expression in ILC3 (gated on alive $CD45^+$ $CD3^-$ $CD127^+$ $ROR\gamma t^+$). (**G**) Distribution of RFP^+ among intestinal ILC3 (gated on $CD3^-$ $CD127^+$ $ROR\gamma t^+$) in percentages (left) and absolute numbers (right). (mean + S.E.M.; n = 15). (**H**) Histograms overlay of the indicated population. *Ncr1*$^+$ (black line) and *Ncr1*^{FM} (light blue) were gated on as described in (C). T cells (grey line) as a negative and positive control for intracellular staining of NKp46 and CD3, respectively.

Figure 2. *Ncr1*^{FM} ILC3 demonstrate elevated IL-22 production and reduced T-bet expression. (**A**). Representative FACS plot of Ki67 versus NKp46 in RFP$^+$ NK1.1$^-$ cells and CD3$^+$ T cells (control). (**B**) Statistical evaluation of Ki67 data obtained from analyses as in (A). (**C**) Representative FACS plot of IL-22 expression by the indicated subsets (among RFP$^+$ NK1.1$^-$) after 4h stimulation with or without IL-23 (50 ng.ml^{-1}). NS = Non Stimulated. (**D**) Percentages of IL-22 positive cells in RFP$^+$ NKp46$^+$ (empty bar) and RFP$^+$ NKp46$^-$ (black bar) (mean + S.E.M.; n=9), *** $p < 0.001$. (**E**) Expression levels (MFI) of intracellular IL-22 protein in unstimulated or IL-23-stimulated cells from the indicated populations. (**F**) Representative FACS plot of IFNγ and IL-22 expression after stimulation with various cytokine mixes as indicated. Of note, cells were first incubated for 1h with IL-1β, IL-2, IL-6, and IL-23 before PMA and ionomycin were added for the remaining 3hrs of incubation. (**G**) Histograms overlay of T-bet expression in RFP$^+$ NK1.1$^+$ (red), RFP$^+$ NKp46$^+$ (grey), RFP$^+$ NKp46$^-$ (light blue) and CD4$^+$ LTi (dark grey). Mean fluorescence intensity (MFI) were normalized to RFP$^+$ NK1.1$^+$ and are displayed in (**H**). (mean + S.E.M.; n=4), ** $p < 0.01$.

Figure 3. Impact of ontogeny and microbiota on *Ncr1*^{FM} ILC3 generation. (**A**) Representative FACS plot of CD4, RFP, NKp46 and GFP expression in ILC3 (gated on alive CD45$^+$ CD3$^-$ CD127$^+$ RORγt$^+$) from the SI-LP of *Ncr1*^{CreGFP} x *Rosa26*^{RFP} mice at the indicated time points. (**B**) Percentages of *Ncr1*$^+$ and *Ncr1*^{FM} ILC3 among NK1.1$^-$ cells, (mean + S.E.M.; $n \geq 9$, **** $p < 0.0001$). (**C**) Percentages of IL-22 positive cells in *Ncr1*$^+$ (empty bar) and *Ncr1*^{FM} (black bar) in SI-LPL from 1 week-old mice (mean + S.E.M.; n=9), ** $p < 0.01$ stimulated or not with IL-23 as indicated. (**D**). Percentages of RORγt$^+$ among CD3$^+$ T cells with or without antibiotic treatment

606 in control (empty bars) or antibiotic treated (black bars) mice (mean + s.d., n = 3), **
607 $p < 0.01$. Antibiotics were administered in drinking water to pregnant mice and mice
608 after birth until sacrifice (6-7 weeks old). (**E**) Representative FACS plot of RFP^+
609 $NK1.1^-$ ILC3 with or without antibiotic treatment. (**F**) Percentages of *Ncr1*$^+$ and
610 *Ncr1*^{FM} ILC3 among $NK1.1^-$ RFP^+ (E) in control (empty bars) or antibiotic treated
611 (black bars) mice (mean + s.d., n = 3).
612
613 **Figure 4. Phenotype and plasticity of *Ncr1*^{FM} ILC3.** (**A**) Representative FACS plot
614 of CD49a and T-bet expression in the indicated ILC3 subsets from the SI-LP of
615 C57BL/6 mice. (**B**) Representative FACS plot of CD49a versus CCR6 expression in
616 *Ncr1*$^+$ (left) and *Ncr1*^{FM} (right) from the SI-LPL of *Ncr1*^{CreGFP} x *Rosa26*^{RFP} mice. (**C**)
617 Representative FACS plot of DNAM-1 versus CD49a and CCR6 expression by cells
618 from the indicated subsets from *Ncr1*^{CreGFP} x *Rosa26*^{RFP} mice. (**D**) $CD45^{int}$ $CD90^{hi}$
619 $NK1.1^-$ $CD49a^+$ GFP^+ were sorted from the SI-LP of *Rag2*$^{-/-}$ *Ncr1*$^{GFP/+}$ mice and
620 cultured on OP9 or OP9-DL1 expressing stromal cells in the presence (grey bar) or
621 absence (black bar) of TGF-β (100 $ng.ml^{-1}$) for up to four days. Mean Fluorescence
622 Intensity (MFI) of GFP in sorted $CD49a^+$ GFP^+ cells was assessed by flow cytometry
623 at the indicated time points. (mean + s.d.; n=3), * $p < 0.05$, ** $p < 0.01$.
624
625

Supplemental Figure Legends

Supplemental Figure 1. Relates to Figure 1. (**A**) Experimental approach for fate-mapping NKp46^{+} cells. (**B**) CD45^{+} RFP+ cells of the indicated organs were stained for NKp46 and NK1.1. Dotplots on the left show NKp46 versus RFP expression of these cells isolated from the indicated organs. Histograms on the right show the expression of NK1.1 by the same cells. BM- bone marrow, SG- salivary glands, aLN- axial lymph nodes, mLN- mesenteric lymph nodes. Histograms overlays show NK1.1 expression by CD19+ cells (grey, negative control) and RFP+ cells (black). (**C**) Analysis of NK1.1, RORγt and NKp46 expression in RFP^{+} cells from the indicated organs in *Ncr1*^{CreGFP} x *Rosa26*^{RFP} mice. First column displayed was gated on alive CD45^{+} RFP^{+}cells. PP : Peyer's Patches; LI-LP : Large Intestine Lamina Propria. (**D**) FACS plots showing the expression of NKp46 versus intracellular Eomes (left) and intracellular RORγt versus intracellular Eomes (right) by CD3-CD19- SI-LP from C57BL/6 mouse.

Supplemental Figure 2. Relates to Figure 1. (**A**) Expression of MHC-II versus CCR6 by the indicated cell populations. (**B**) Expression of CD4 versus CCR6 by the indicated cell populations.

Supplemental Figure 3. Relates to Figure 2. (**A**) Related to Figure 2F. Intracellular IL-22 versus GM-CSF expression by the indicated cell populations and stimulated as indicated. Cells were stimulated as detailed in figure legend 2F. (**B**) SI-LPL from *Ncr1*^{CreGFP} x *Rosa26*^{RFP} mice were stimulated for 4hrs with PMA and ionomycin and then stained for intracellular IL-17. Shown are IL-17 versus RFP (left; of note, there

650 are no double positive cells) and IL-17 versus CD3 (right; 25% of $CD3^+$ cells express
651 IL-17).
652
653 Supplemental Figure 4. Relates to Figure 3A. (**A**)FACS plots showing the expression
654 of NKp46 and NK1.1 by total RFP+ cells (left) and ILC3 (right) in E18.5 fetal livers.
655 (**B**) Representative FACS plots of expression of CCR6 and CD49a by cells cultured
656 for 4 days on OP9 feeder cells with or without the Notch-logand DL-1 and with or
657 without TGFβ as indicated. Grey overlay represents RFP^-CCR6^+ ILC3, red - *Ncr1*$^+$
658 ILC3, blue overlay represents *Ncr1*^{FM} ILC3.

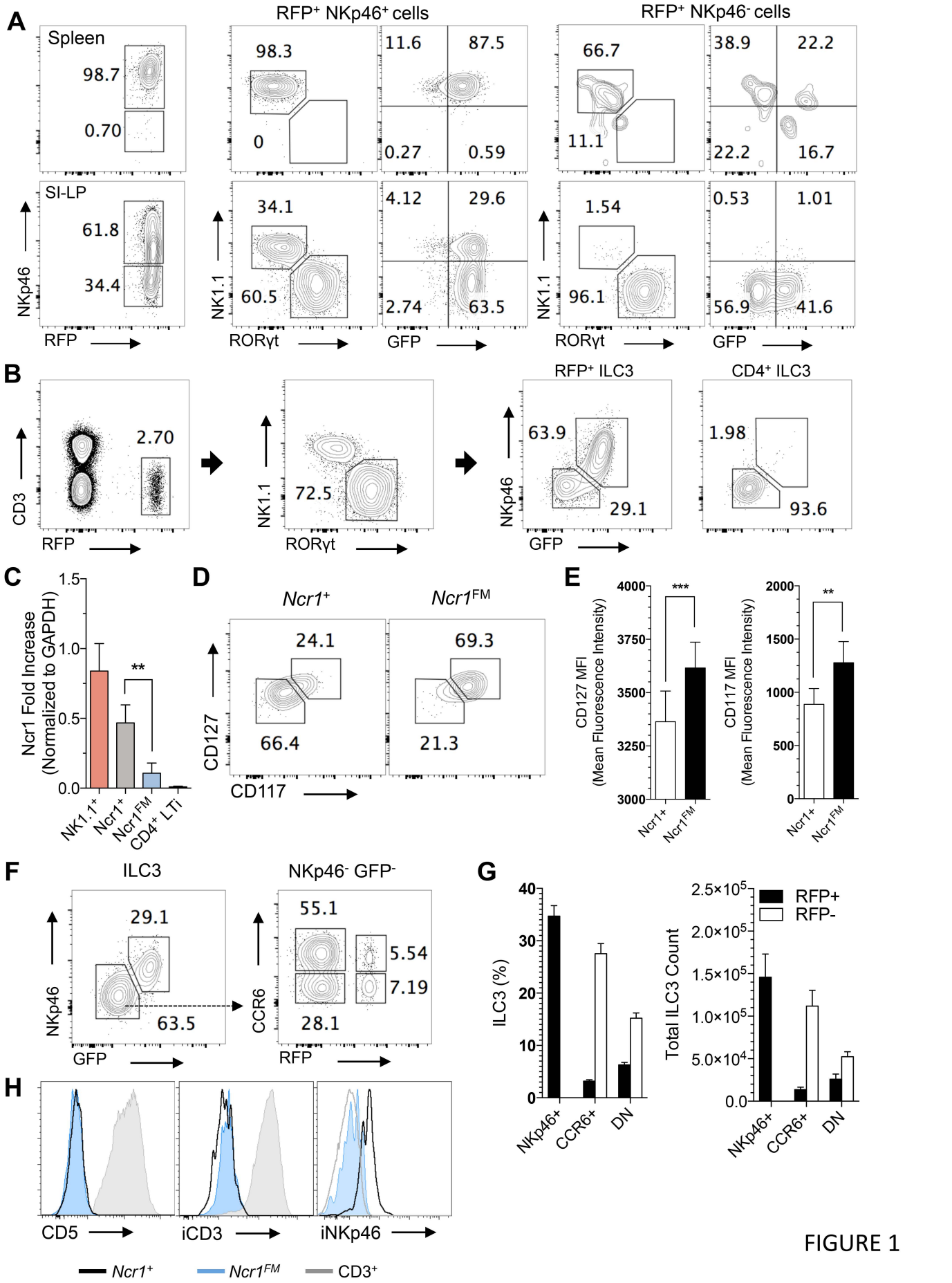
A
Spleen
98.7
0.70
SI-LP
61.8
34.4
NKp46
RFP
RFP+ NKp46+ cells
98.3
0
11.6
87.5
0.27
0.59
34.1
60.5
4.12
29.6
2.74
63.5
NK1.1
RORγt
GFP
RFP+ NKp46- cells
66.7
11.1
38.9
22.2
22.2
16.7
1.54
96.1
0.53
1.01
56.9
41.6
B
CD3
2.70
RFP
72.5
RFP+ ILC3
63.9
29.1
CD4+ ILC3
1.98
93.6
C
Ncr1 Fold Increase (Normalized to GAPDH)
1.5
1.0
0.5
0.0
**
NK1.1+
Ncr1+
Ncr1FM
CD4+ LTi
D
Ncr1+
Ncr1FM
24.1
66.4
69.3
21.3
CD127
CD117
E
CD127 MFI (Mean Fluorescence Intensity)
4000
3750
3500
3250
3000
***
Ncr1+
Ncr1FM
CD117 MFI (Mean Fluorescence Intensity)
2000
1500
1000
500
0
**
F
ILC3
29.1
63.5
NKp46
GFP
NKp46- GFP-
55.1
5.54
7.19
28.1
CCR6
RFP
G
ILC3 (%)
40
30
20
10
0
NKp46+
CCR6+
DN
Total ILC3 Count
2.5×10^5
2.0×10^5
1.5×10^5
1.0×10^5
5.0×10^4
0.0
RFP+
RFP-
H
CD5
iCD3
iNKp46
Ncr1+
Ncr1FM
CD3+

FIGURE 1

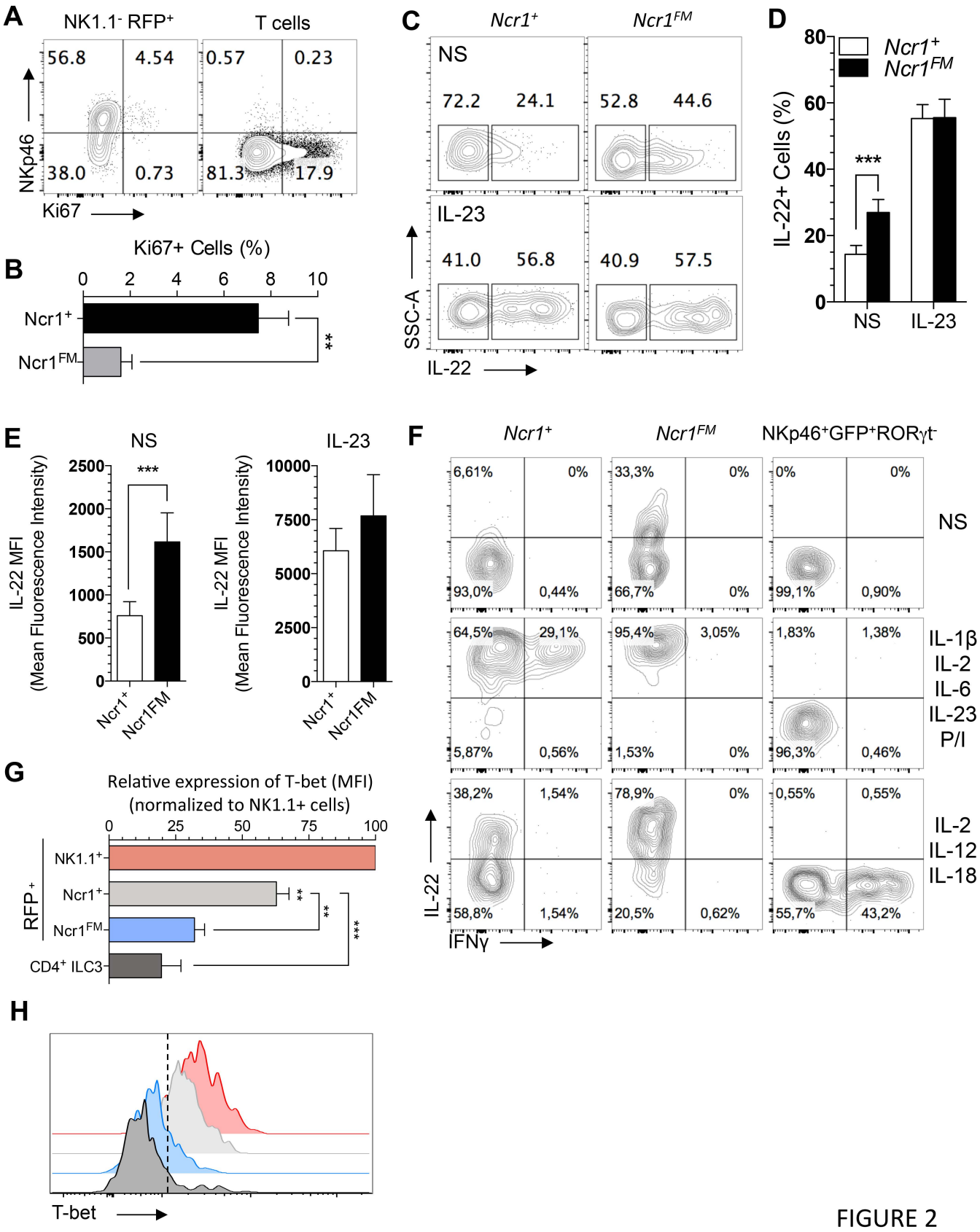
A
NK1.1- RFP+
T cells
56.8
4.54
0.57
0.23
38.0
0.73
81.3
17.9
NKp46
Ki67
B
Ki67+ Cells (%)
0
2
4
6
8
10
Ncr1+
Ncr1FM
**
C
Ncr1+
Ncr1FM
NS
72.2
24.1
52.8
44.6
IL-23
41.0
56.8
40.9
57.5
SSC-A
IL-22
D
Ncr1+
Ncr1FM
IL-22+ Cells (%)
80
60
40
20
0
***
NS
IL-23
E
NS
IL-23
IL-22 MFI
(Mean Fluorescence Intensity)
2500
2000
1500
1000
500
0
***
10000
7500
5000
2500
0
Ncr1+
Ncr1FM
F
Ncr1+
Ncr1FM
NKp46+GFP+RORγt-
6,61%
0%
0%
0%
33,3%
0%
0%
0%
93,0%
0,44%
66,7%
0%
99,1%
0,90%
NS
64,5%
29,1%
95,4%
3,05%
1,83%
1,38%
IL-1β
IL-2
IL-6
IL-23
P/I
5,87%
0,56%
1,53%
0%
96,3%
0,46%
38,2%
1,54%
78,9%
0%
0,55%
0,55%
IL-2
IL-12
IL-18
58,8%
1,54%
20,5%
0,62%
55,7%
43,2%
IL-22
IFNγ
G
Relative expression of T-bet (MFI)
(normalized to NK1.1+ cells)
0
25
50
75
100
RFP+
NK1.1+
Ncr1+
Ncr1FM
CD4+ ILC3
**
**
***
H
T-bet

FIGURE 2

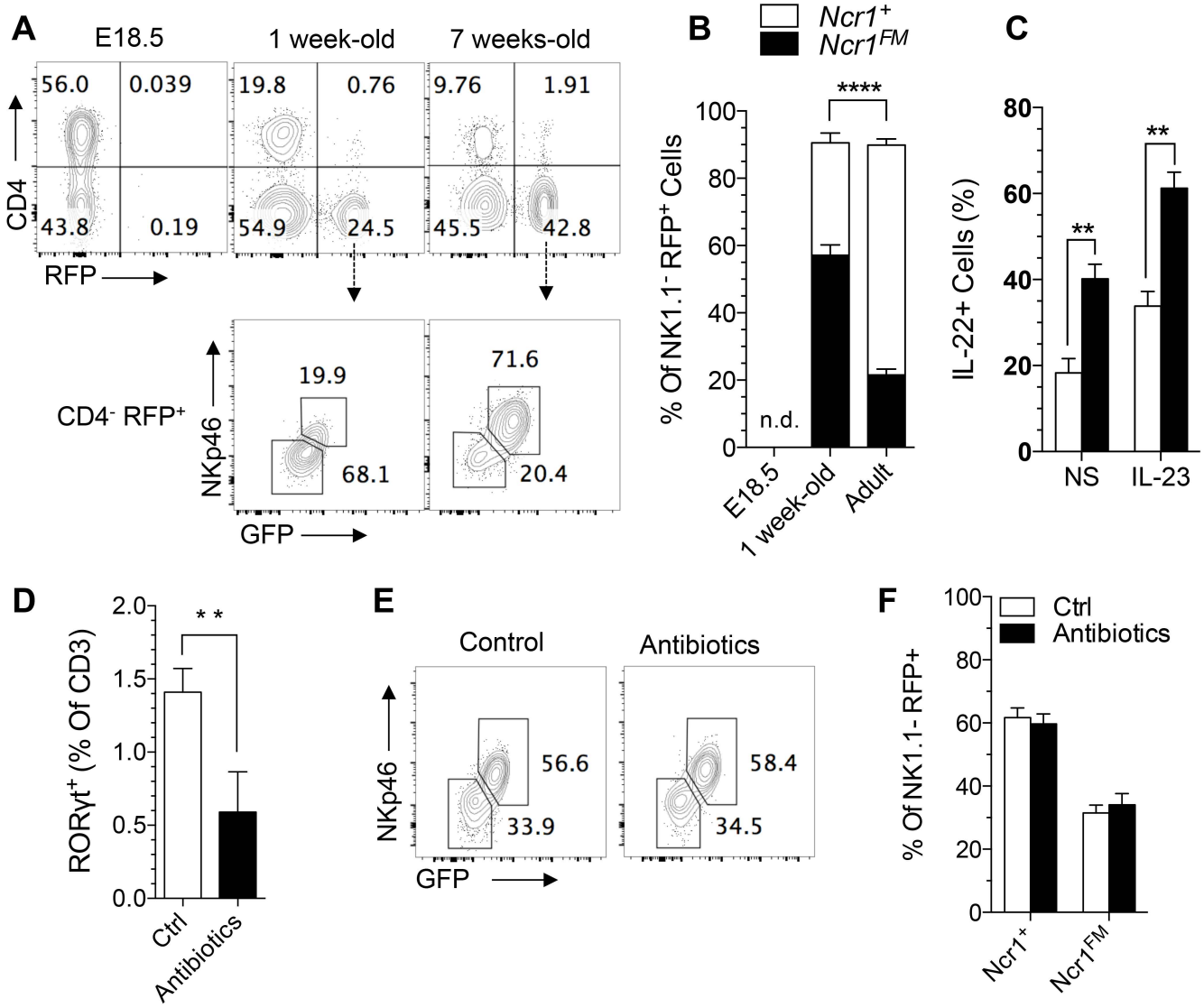
A
E18.5
1 week-old
7 weeks-old
56.0
0.039
43.8
0.19
19.8
0.76
54.9
24.5
9.76
1.91
45.5
42.8
CD4
RFP
CD4- RFP+
NKp46
GFP
19.9
68.1
71.6
20.4
B
Ncr1+
Ncr1FM
****
% Of NK1.1- RFP+ Cells
n.d.
E18.5
1 week-old
Adult
C
**
**
IL-22+ Cells (%)
NS
IL-23
D
**
RORγt+ (% Of CD3)
Ctrl
Antibiotics
E
Control
Antibiotics
NKp46
GFP
56.6
33.9
58.4
34.5
F
Ctrl
Antibiotics
% Of NK1.1- RFP+
Ncr1+
Ncr1FM

FIGURE 3

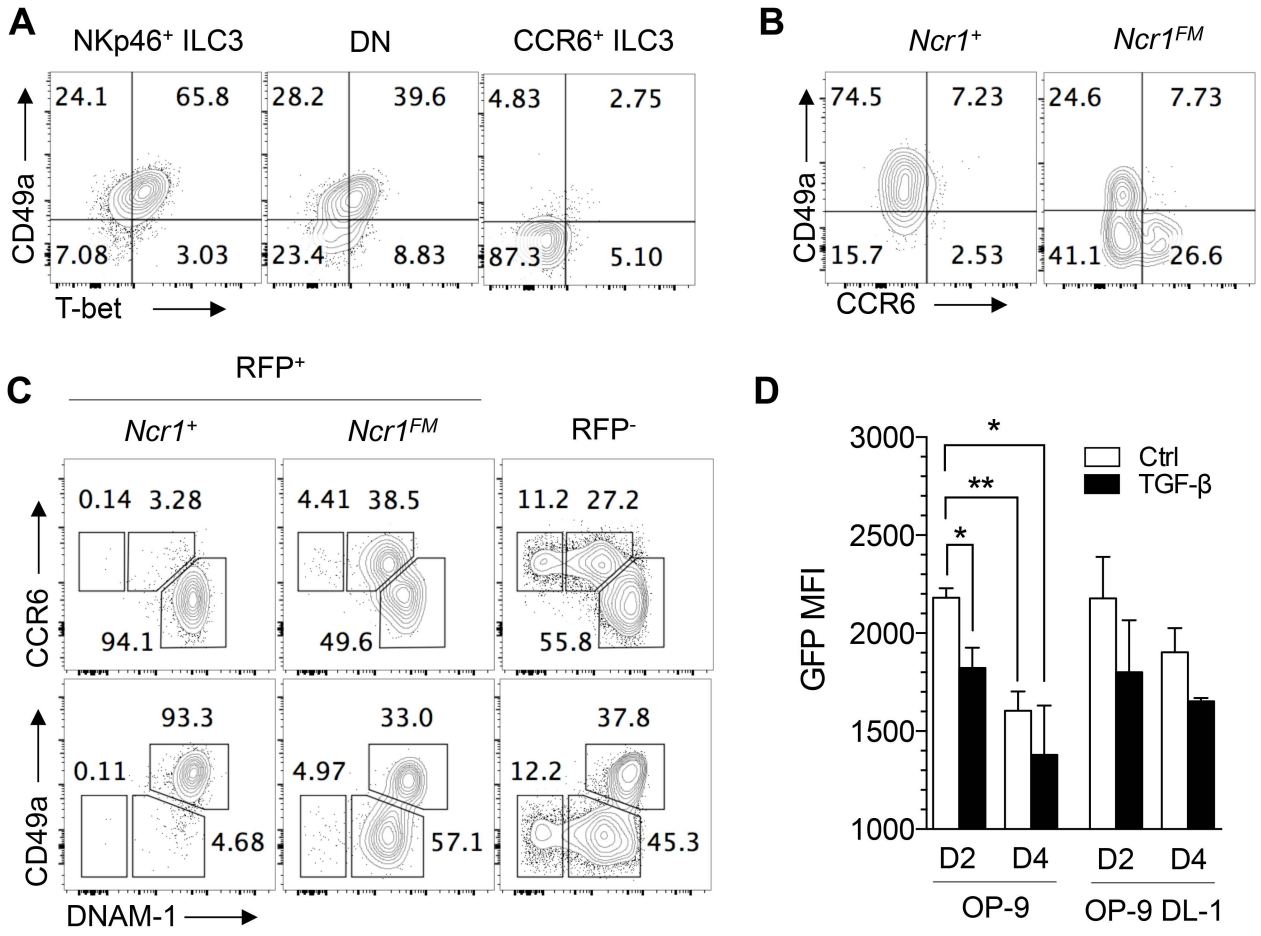
A
NKp46+ ILC3
DN
CCR6+ ILC3
24.1
65.8
7.08
3.03
28.2
39.6
23.4
8.83
4.83
2.75
87.3
5.10
CD49a
T-bet
B
Ncr1+
Ncr1FM
74.5
7.23
15.7
2.53
24.6
7.73
41.1
26.6
CD49a
CCR6
C
RFP+
Ncr1+
Ncr1FM
RFP-
0.14
3.28
94.1
4.41
38.5
49.6
11.2
27.2
55.8
CCR6
93.3
0.11
4.68
33.0
4.97
57.1
37.8
12.2
45.3
CD49a
DNAM-1
D
GFP MFI
3000
2500
2000
1500
1000
*
**
*
Ctrl
TGF-β
D2
D4
D2
D4
OP-9
OP-9 DL-1

FIGURE 4

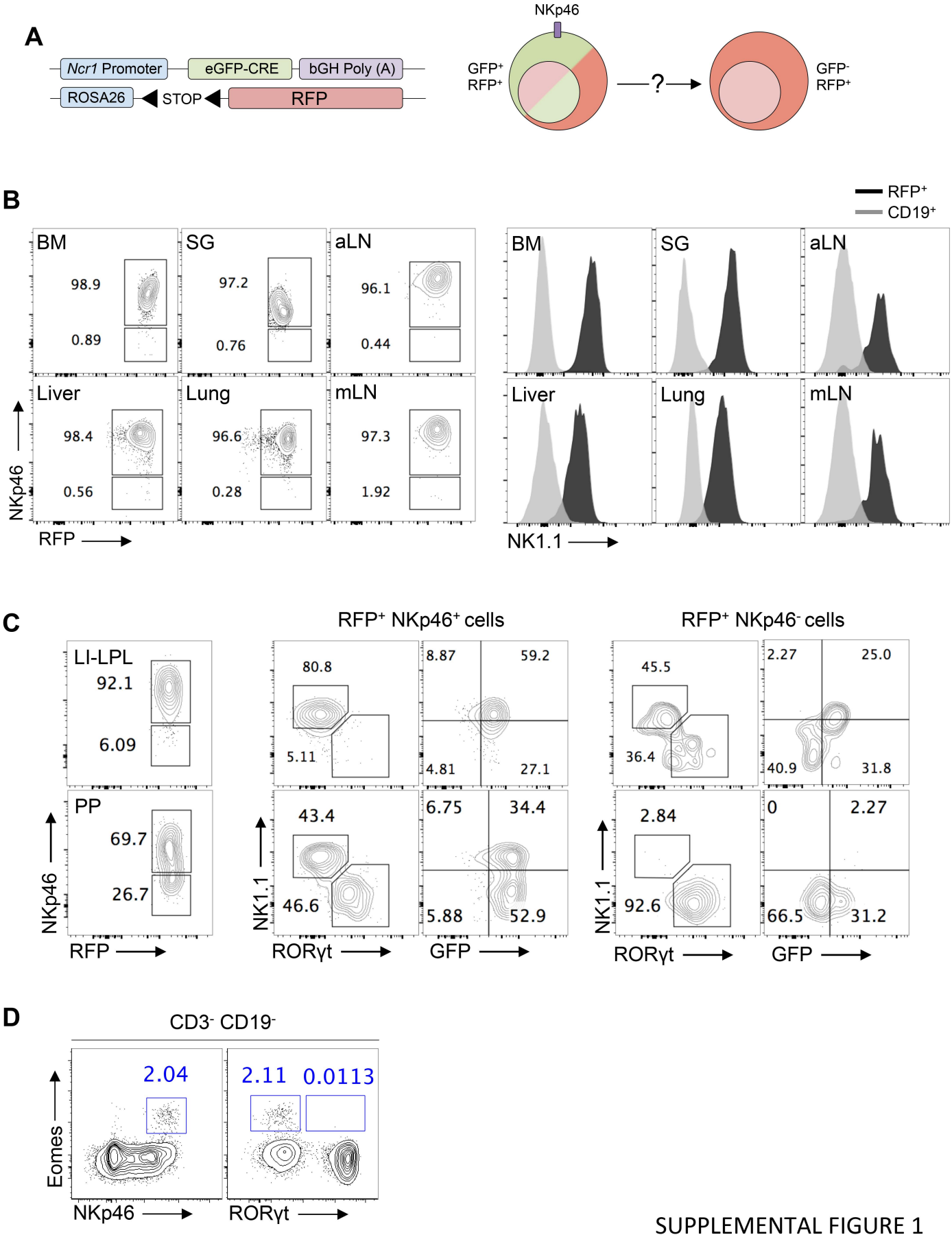

SUPPLEMENTAL FIGURE 1

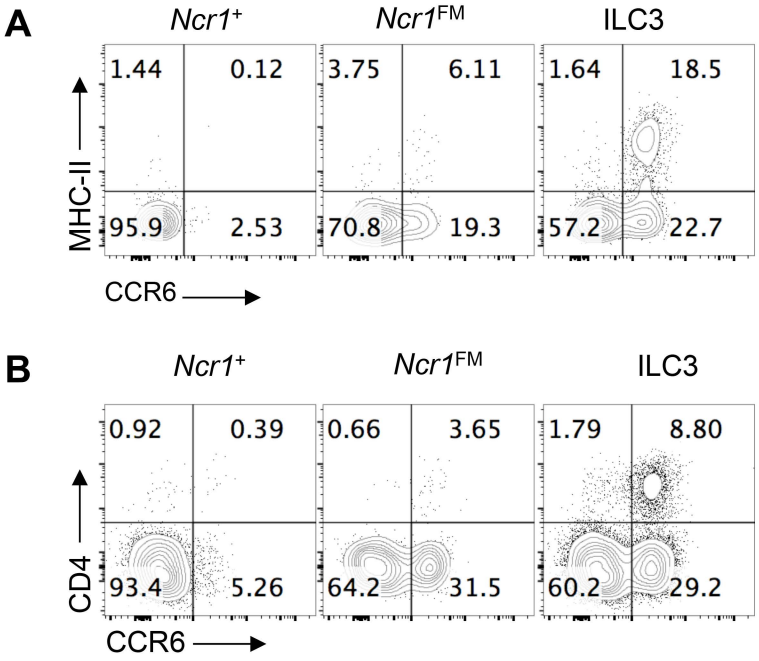

SUPPLEMENTAL FIGURE 2

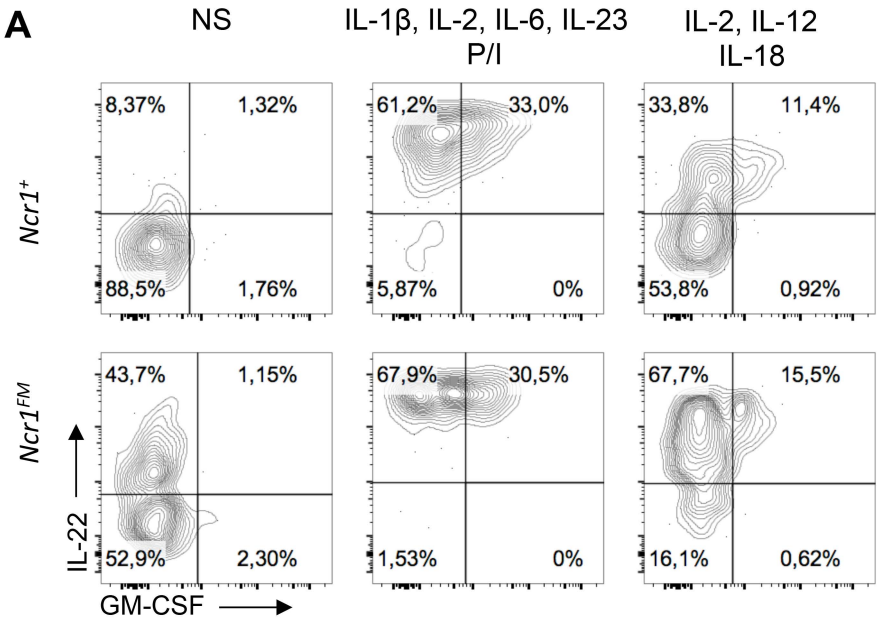

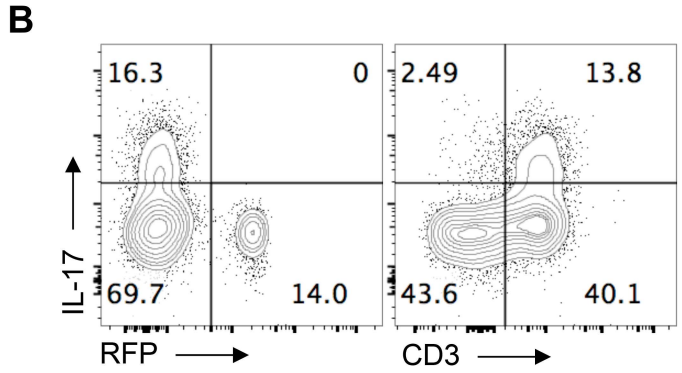

SUPPLEMENTAL FIGURE 3

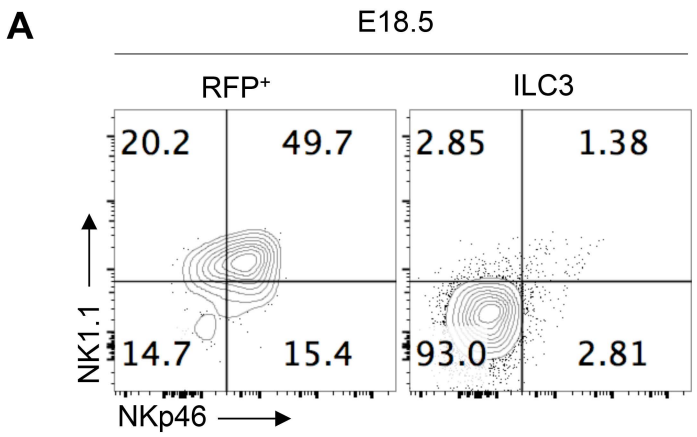

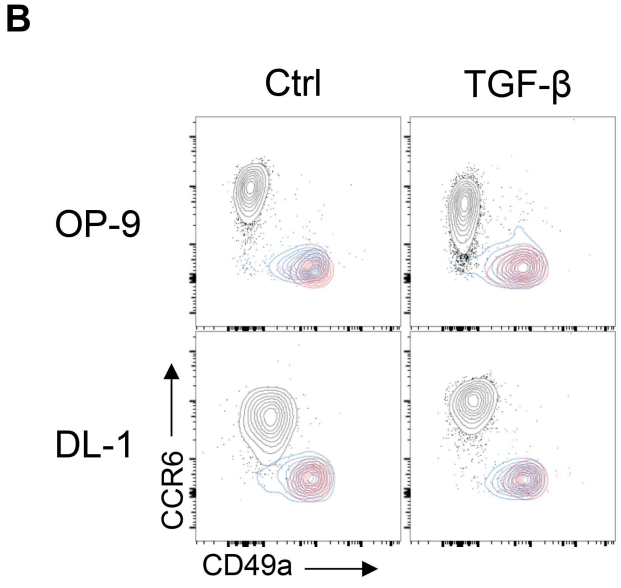

SUPPLEMENTAL FIGURE 4